COMPUTED TOMOGRAPHY OF CHEMILUMINESCENCE USING A SPARSE SENSING FRAMEWORK

A. Procacci*,, R. Amaduzzi*,**, A. Coussement*,**, A. Parente*,****
alberto.procacci@ulb.be
*Aero-Thermo-Mechanics Department, Université Libre de Bruxelles, Av. Franklin Roosevelt 50, Bruxelles, 1050, Belgium
**Brussels Institute for Thermal-Fluid Systems and Clean Energy (BRITE), Université Libre de Bruxelles and Vrije Universiteit Brussel, Pleinlaan 2, Bruxelles, 1050, Belgium

Abstract
The aim of this work is to demonstrate the use of sparse sensing for the prediction of the 3D chemiluminescence field of a flame from the line-of-sight integrated chemiluminescence signal. Sparse sensing is a machine-learning technique that leverages the intrinsic low-dimensionality of physical phenomena to predict the state of the system given few measurements. This makes it a good candidate to be employed in Computed Tomography of Chemiluminescence (CTC), an imaging technique used to reconstruct the 3D chemiluminescence field from chemiluminescence images. The methodology is demonstrated on a virtual experiment based on the data coming from the Large Eddy Simulation of a jet flame in a vitiated coflow, where OH is employed as a surrogate of OH*.

Introduction
Combustion technologies will have to drastically reduce their carbon emissions by adopting zero-carbon fuels to meet the objective set by the European Commission [1]. The introduction of these fuels involves a radical change in the design and operation of combustion system, and the short timeline for the development of these new technologies does not allow a traditional trial-and-error approach.
Luckily, the advancement in combustion modelling [2,3], as well as the development of new diagnostic techniques [4], have produced a set of tools that can be used for the rapid design and validation of new combustion systems. However, these cannot always be transferred from lab-scale to industrial applications.
A simpler diagnostic tool that is extensively used in industrial applications is chemiluminescence [5]. Chemiluminescence is a phenomenon in which light is emitted from excited species produced by chemical reactions. In the context of combustion, chemiluminescence is often associated with the excited species OH* and CH* [6]. The advantage of chemiluminescence over laser diagnostics is that it does not require an external light source, and thus can be employed also when the optical access is limited. The downside lies in the fact that the signal is line-of-sight integrated, resulting in incomplete information about the 3D distribution of the

chemiluminescent sources. To reconstruct the 3D chemiluminescence field, the Computed Tomography of Chemiluminescence (CTC) is generally employed [7]. CTC generally involves the acquisition of multiple 2D chemiluminescence images at different viewing angles, which are combined using tomographic reconstruction algorithms to generate a 3D representation of the chemiluminescence field.
The goal of this paper is to first develop such an algorithm based on sparse sensing, and then to demonstrate its capability by reconstructing the 3D OH field from 2D OH images. Sparse sensing is a machine-learning technique that exploits the intrinsic low-dimensional representation of physical, to predict the state of the system using few measurements. The mathematical framework of sparse sensing was developed by Candes and Tao [8], and techniques for the selection of the optimal sensors' placement were developed by Manohar et al. [9]. Recently, we have successfully applied sparse sensing to the prediction of the 3D temperature field of the ULB furnace given few temperature measurements [10].

Computed tomography of chemiluminescence
The CTC problem is essentially an inversion problem in which the objective is to reconstruct the 3D field $\boldsymbol{f}(x_f, y_f, z_f)$, given its projection on the camera sensor $\boldsymbol{p}(x_p, y_p)$ and the point spread function $\boldsymbol{C}(x_f, y_f, z_f, x_p, y_p)$ that relates the amount of light produced by a point source onto the sensor's plane:

$$\boldsymbol{p} = \boldsymbol{C}\boldsymbol{f} \tag{1}$$

Figure 1 shows a schematic representation of the CTC mathematical framework. In computed tomography, $\boldsymbol{f}$ is usually discretized into n voxels and the light emitted from each voxel is focused by the camera system onto the sensor's plane.
The size s of $\boldsymbol{p}$ depends on the number of pixels in the x_p and y_p directions, as well as on the number of images such that $s = n_{x_p} \times n_{y_p} \times n_i$.
The point spread function depends only on the position and characteristics of the camera system. The computation of $\boldsymbol{C}$ is essentially a ray-tracing problem, where the objective is to compute the path of the light from the source to the observer.
The size of $\boldsymbol{C}$ can quickly become computationally challenging. For example, if the system is discretized using $n = 64 \times 64 \times 64$ and the resolution of the sensor is 512×512 with 5 cameras installed, the size of $C = s \times n = 389120 \times 262144$.

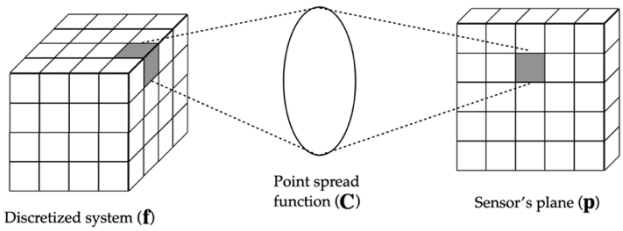

Figure 1. Schematic representation of the CTC mathematical framework.

Sparse sensing

Sparse sensing assumes that physical phenomena admit a low-dimensional representation in a transforming basis. This fact can be leveraged to achieve the prediction of the system's state using a small set of sensors.

The first step in the sparse sensing algorithm is to reduce the dimensionality of the system's state $\boldsymbol{f}$ by finding a transforming basis $\boldsymbol{\Phi}$, such that:

$$\boldsymbol{f} = \boldsymbol{\Phi}\boldsymbol{\psi} \tag{2}$$

where the size r of the low-dimensional vector $\boldsymbol{\psi}$ is much smaller than n.

An obvious choice for computing the transforming basis is to use the Proper Orthogonal Decomposition (POD) [11], because it ensures that the r-order truncation minimizes the l_2 norm reconstruction error.

To compute the POD basis, we can employ the Singular Value Decomposition (SVD):

$$\boldsymbol{F}(r,t) = \boldsymbol{U}(r)\boldsymbol{\Sigma}\boldsymbol{V}^T(t) \tag{3}$$

The matrix $\boldsymbol{F}$ contains m system's states $\boldsymbol{f}$ arranged as column vectors. In our case, $\boldsymbol{F}$ includes multiple timesteps of the 3D chemiluminescence field. The matrix $\boldsymbol{U}$ contains the spatial modes, while the matrix $\boldsymbol{V}$ contains the POD temporal coefficients. The matrix $\boldsymbol{\Sigma}$ is a diagonal matrix containing the singular values, which are a measure of the amount of information captured by each mode.

The linear system in Eq. 1 can be then rewritten as:

$$\boldsymbol{p} = \boldsymbol{C}\boldsymbol{f} = \boldsymbol{C}\boldsymbol{U}\boldsymbol{a} = \boldsymbol{\Theta}\boldsymbol{a} \tag{4}$$

where $\boldsymbol{a}$ is the low-dimensional POD projection of $\boldsymbol{f}$. The matrix $\boldsymbol{\Theta}$ has dimensions $s \times r$, and the conditioning number of this matrix is much lower than the conditioning number of the matrix $\boldsymbol{C}$, provided that some conditions between the placement of sensors with respect to the POD modes are met [12]. This means that the new linear system can be solved by inverting the matrix $\boldsymbol{\Theta}$, using conventional approaches such as least-squares regression.

To improve the prediction accuracy of the low-dimensional projection, physical constraints such as positivity can be introduced, so that the constrained objective function becomes:

$$\begin{aligned} \boldsymbol{a}* = \ & \underset{\boldsymbol{a}}{\operatorname{argmin}} \, || \, \boldsymbol{y} - \boldsymbol{\Theta}\boldsymbol{a} ||_2^2 \\ & \boldsymbol{s.t.} \quad \mathbf{U}_r\boldsymbol{a} > 0 \end{aligned} \tag{5}$$

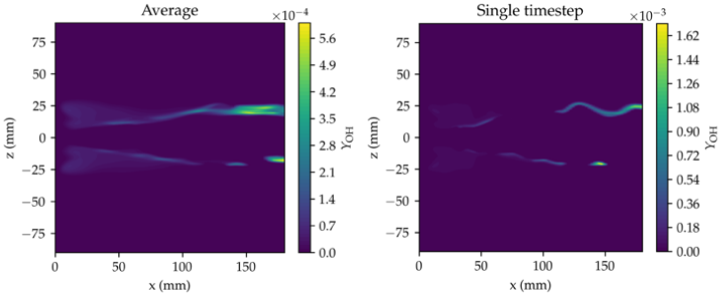

Figure 2. Average and instantaneous OH mass fraction distribution.

Numerical dataset

The numerical dataset comes from the 3D Large Eddy Simulation (LES) of the Jet in Hot Coflow (JHC). The OpenFOAM based, finite-rate solver FiReSMOKE is employed for the simulation. The code solves Favre-filtered mass, momentum and energy conservation equations along with the filtered transport equations for the species. The filtered species source terms are determined from the Partially-Stirred Reactor (PaSR) turbulence-chemistry interaction model [3]. The PaSR model separates each computational cell into a reactive structure where combustion takes place and a surrounding fluid where only mixing occurs.

The simulation domain includes the first 180 mm downstream of the fuel jet exit in the axial direction and 90 mm in the radial direction from the centerline. The domain is discretized as a 3D cylinder structured mesh made of approximately 1.5M cells. We generate inlet turbulence for all three streams using the LEMOS inflow generation method [13]. The inlet profiles for temperature and H_2O, CO_2 and O_2 mass fractions are taken from the experimental measurements in Dally et al. [14].

The kinetic mechanism employed for the detailed reference simulation is the GRI3.0 without the NOx sub-mechanism. It consists of 36 species and 219 reactions. The minimum turbulent kinetic energy resolved in the grid is 80% in every cell and above 90% in most locations of interest.

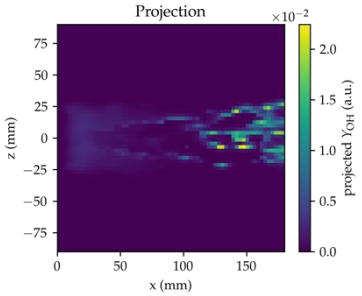

Figure 3. Projection of the instantaneous OH mass fraction distribution on the sensor's plane (p).

Results

The dataset contains 61 timesteps, of which the first 60 were employed as training data to build the POD modes matrix $\boldsymbol{U}$, while the last timestep was used to test the sparse sensing model.

Figure 2 shows the average and instantaneous (last timestep) OH mass fraction distribution. Before computing the SVD, the dataset has been downscaled and interpolated on a $64 \times 64 \times 64$ regular grid, where each voxel has a volume equal to around $22\ \mathrm{mm}^3$.

Figure 3 shows the projection p on the sensor's plane for the last timestep, which is used as input to the sparse sensing model in Equation 4. The obtained prediction is

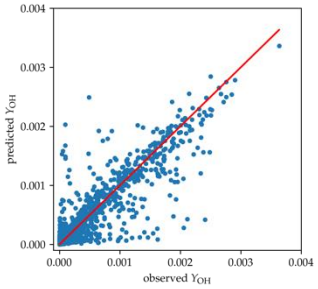

Figure 4. Parity plot of the observed and predicted OH mass fraction distribution. The red line indicates the perfect correlation.

compared to the observed OH mass distribution in the parity plot shown in Figure 4. The prediction is overall accurate with a coefficient of determination $R^2 \approx 0.9$. The comparison between the observed and predicted OH mass distribution for different slices is shown in Figure 5. The model sometimes underpredict or overpredict the pixel values, but the overall distribution is remarkably close to the original one.

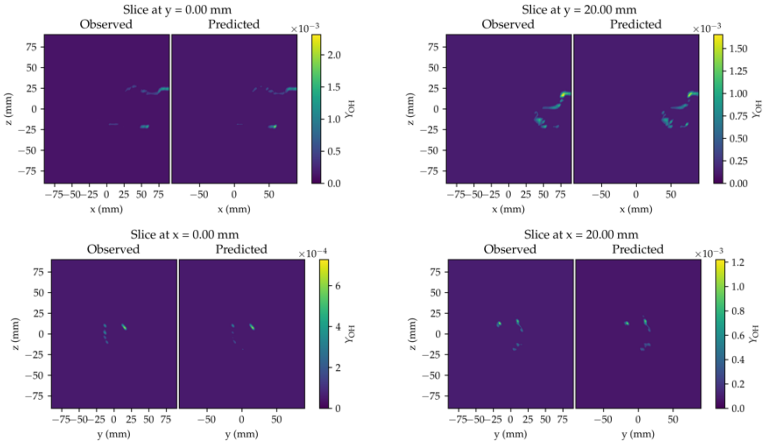

Figure 5. Comparison between the observed and predicted OH mass fraction for different slices.

Conclusions

This work demonstrates how to employ a sparse sensing framework to solve the CTC problem. A 3D LES of the JHC has been used as a synthetic dataset, and the OH mass fraction distribution has been employed as a surrogate for the OH* chemiluminescence signal. The results show that the model can predict the 3D OH field with good accuracy using a single projection, which is much less than what is

generally needed for conventional CTC techniques. This indicates that the proposed technique could be also applied on industrial experiments with very limited optical access. The next step will be to validate this technique on experimentally measured chemiluminescence emissions.

References

[1] European Commission, “A Hydrogen Strategy for a climate neutral Europe” July, 2020.

[2] A. Giusti and E. Mastorakos, “Turbulent Combustion Modelling and Experiments” Flow, Turbul. Combust., vol. 103, no. 4, pp. 847–869, 2019.

[3] A. Péquin, S. Iavarone, R. Malpica Galassi, and A. Parente, “The partially stirred reactor model for combustion closure in large eddy simulations: Physical principles, sub-models for the cell reacting fraction, and open challenges,” Phys. Fluids, vol. 34, no. 5, 2022.

[4] K. Kohse-Höinghaus, R. S. Barlow, M. Aldén, and J. Wolfrum, “Combustion at the focus: Laser diagnostics and control,” Proc. Combust. Inst., vol. 30, no. 1, pp. 89–123, 2005.

[5] M. J. Bedard, T. L. Fuller, S. Sardeshmukh, and W. E. Anderson, “Chemiluminescence as a diagnostic in studying combustion instability in a practical combustor,” Combust. Flame, vol. 213, pp. 211–225, 2020.

[6] A. Procacci, M. Cafiero, S. Sharma, M. M. Kamal, A. Coussement, and A. Parente, “Digital Twin for Experimental Data Fusion Applied to a Semi-Industrial Furnace Fed with H2-Rich Fuel Mixtures,” Energies, vol. 16, no. 2, pp. 1–14, 2023.

[7] X. Li and L. Ma, “Capabilities and limitations of 3D flame measurements based on computed tomography of chemiluminescence,” Combust. Flame, vol. 162, no. 3, pp. 642–651, 2015.

[8] E. J. Candes and T. Tao, “Near-optimal signal recovery from random projections: Universal encoding strategies?,” IEEE Trans. Inf. Theory, vol. 52, no. 12, pp. 5406–5425, 2006.

[9] K. Manohar, B. W. Brunton, J. N. Kutz, and S. L. Brunton, “Data-Driven Sparse Sensor Placement for Reconstruction,” 2017.

[10] A. Procacci, R. Amaduzzi, A. Coussement, and A. Parente, “Adaptive digital twins of combustion systems using sparse sensing strategies,” Proc. Combust. Inst., 2022.

[11] G. Berkooz, P. Holmes, and J. L. Lumley, “The proper orthogonal decomposition in the analysis of turbulent flows,” Annu. Rev. Fluid Mech., vol. 25, no. 1, pp. 539–575, 1993.

[12] S. L. Brunton and J. N. Kutz, Data-Driven Science and Engineering: Machine Learning, Dynamical Systems, and Control. Cambridge University Press, 2019.

[13] N. Kornev, H. Kröger, and E. Hassel, “Synthesis of homogeneous anisotropic turbulent fields with prescribed second-order statistics by the random spots method,” Commun. Numer. Methods Eng., vol. 24, no. 10, pp. 875–877, 2008.

[14] B. B. Dally, A. N. Karpetis, and R. S. Barlow, “Structure of turbulent non-premixed jet flames in a diluted hot coflow,” Proc. Combust. Inst., vol. 29, no. 1, pp. 1147–1154, 2002.